LANGMUIR

pubs.acs.org/Langmuir Article

Probing the Hydrogen Bond Involving Acridone Trapped in a Hydrophobic Biological Nanocavity: Integrated Spectroscopic and Docking Analyses

Brotati Chakraborty,* Chaitrali Sengupta, Uttam Pal, and Samita Basu

Cite This: https://dx.doi.org/10.1021/acs.langmuir.9b03506 Read Online

ACCESS | Metrics & More | Article Recommendations | Supporting Information

ABSTRACT: Spectroscopic analyses reveal that acridone (AD) penetrates through the structure and enters the hydrophobic cavity of the protein β-lactoglobulin (βLG). Although the protein contains two tryptophan (Trp) residues, AD interacts with only one (Trp-19), which is authenticated by the appearance of a single isoemissive point in TRANES. Alteration in the secondary structure of the protein while AD pierces through βLG is evident from the circular dichroism spectroscopic study. The ground-state interaction between AD and βLG is proven from the UV−vis spectroscopic study and the static nature of quenching of intrinsic fluorescence of the protein by the ligand. The steady-state fluorescence study in varied temperatures indicates the involvement of hydrogen bonding in the ligand−protein interaction. Further, the time-resolved fluorescence anisotropy study gives a hint of the presence of a hydrogen bond in AD−βLG interaction, which possibly involves the rotamers of Trp-19. In fact, the idea of involvement of rotamers of Trp-19 is obtained from the increase in fluorescence lifetime of βLG in the presence of AD. The docking study agrees to the involvement of hydrogen bonding in AD−βLG interaction. The direct evidence of hydrogen bonding between Trp and AD is obtained from the laser flash photolysis studies where the signature of formation of $ADH^{\bullet}$ and $Trp^{\bullet}$ through hydrogen abstraction between Trp and AD, loosely bound through hydrogen bonding, gets prominence. Thus, binding of AD to βLG involves hydrogen bonding in a hydrophobic pocket of the protein.

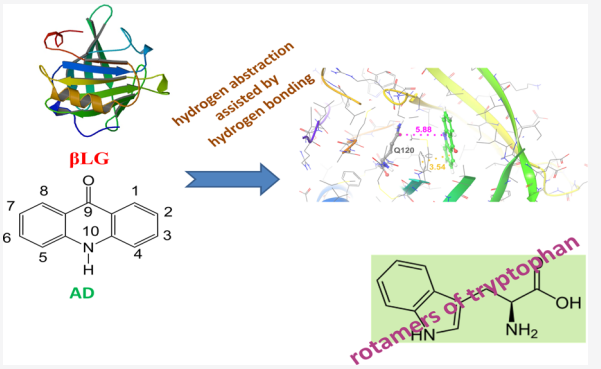

INTRODUCTION

β-Lactoglobulin (βLG) is a food-based biopolymer, which is the most abundant protein in the whey fraction of milk of cow, sheep, and other mammalians and responsible for transport of hydrophobic nutrients.[1−5] It is a small globular protein (molecular weight 18.3 kDa) containing 162 amino acid residues, folded into a calyx formed by eight antiparallel β-strands and an α-helix located at the outer surface of the β-barrel.[6] Several reports suggest that there are at least two hydrophobic binding sites in the βLG, one in the internal cavity and the other on the outer surface located between the β-barrel and the α-helix.[6] βLG serves as a model protein as its conformation, function, and physiological properties are well-defined. Further, it has two tryptophan (Trp) residues in varied microenvironments, viz. Trp-19 and Trp-61,[6] and thus, the intrinsic fluorescence of Trp may be utilized for the spectroscopic study of the protein.

Acridine derivatives are known to interact with DNA,[7−11] and some of them are recognized as prospective candidates of photosensitizers in photodynamic therapy.[12−14] Thus, study of interactions of such acridine derivatives with exogenous and endogenous drug-delivery vehicles is of pharmacological importance. Previously, we have reported the interactions of an acridine derivative, acridone (AD), as depicted in Figure 1, with two model with two model proteins, human serum albumin (HSA)[15] and bovine serum albumin (BSA).[16] HSA consists of a single Trp (Trp-214) residue, which is housed in a hydrophobic cavity, whereas, BSA contains two Trp residues (Trp-212 and Trp-134) between which Trp-212 resides in a hydrophobic pocket while Trp-134 is solvent exposed. We have observed that in case of AD−HSA interaction, AD directly interacts with Trp-214 while in case of AD−BSA

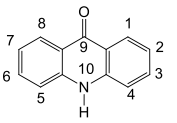

Figure 1. Chemical structure of AD.

Received: November 10, 2019
Revised: December 22, 2019
Published: January 17, 2020

interaction, AD initially gets hooked to Trp-212 inducing strong conformational changes in the protein, which finally paves its way to reach Trp-134. Thus, the common phenomenon for both the cases is that AD initially has a tendency to approach the hydrophobic pocket of the protein. Also, both these systems involve photoinduced electron transfer (PET) from the Trp residues of the proteins to AD.

Thus, we have decided to choose another model protein that has more than one Trp residue in varied environments and make an attempt to study its interaction with AD to verify whether the acridine derivative can interact with all the Trp residues similar to AD−BSA interaction or selectively probe the microenvironment around a particular Trp residue, depending on the nature of the protein. Accordingly, we have selected βLG as our model protein as it contains two Trp residues in diverse microenvironments, viz. Trp-19 residing in an apolar environment and Trp-61 being partly exposed to the solvent.[6] In the present communication, we have investigated the nature of binding interaction of AD with βLG using spectroscopic methods as well as docking study. It is interesting to note that AD primarily houses itself in a hydrophobic cavity of the protein, and hydrogen bonding plays a pivotal role in the binding interaction, which is detected mainly by fluorescence and laser flash photolysis (LFP) studies. Contrary to AD−serum albumin systems, PET is not prevalent in the AD−βLG system, rather hydrogen abstraction assisted by hydrogen bonding is found to occur.

EXPERIMENTAL METHODS

Materials. AD was procured from Fluka. Stock solution of AD was prepared in UV spectroscopy-grade ethanol, which was procured from Spectrochem. βLG was purchased from Sigma. Apart from the stock solution of AD, all other solutions were prepared in 10 mM Tris-HCl buffer of pH 7.4.

Apparatus. *Circular Dichroism Spectroscopy.* Circular dichroism (CD) spectra were recorded in a Jasco J-815 CD spectropolarimeter using a 1 mm path length quartz cuvette. For each spectrum, three consecutive readings were averaged at a constant temperature of 298 K.

Absorption Spectroscopy. A Jasco V-650 absorption spectrophotometer was utilized for recording UV−vis absorption spectra using a pair of 1 × 1 cm quartz cuvettes at 298 K. Concentration of βLG was determined spectrophotometrically using the value of molar extinction coefficient of the protein at 280 nm as 17 600 M^{-1} cm^{-1}.[17]

Fluorescence Spectroscopy. A Spex Fluoromax-3 spectrophotofluorimeter was utilized for recording steady-state fluorescence spectra using a 1 × 1 cm quartz cuvette at 298, 303 and 308 K with an excitation wavelength of 280 nm. The fluorescence of βLG was corrected for inner filter effect, owing to the absorbance of AD at the excitation and emission wavelengths using the following equations[18]

$$F_{corr} = F_{obs} \times \text{antilog}\left(\frac{OD_{ex} + OD_{em}}{2}\right) \quad (1)$$

where F_{corr} and F_{obs} are the corrected and observed fluorescence intensities, respectively, and OD_{ex} and OD_{em} are the absorbances at excitation and emission wavelengths, respectively. A Jobin Yvon Horiba picoseconds-resolved time-correlated single photon-counting (TCSPC) spectrometer was used to measure fluorescence lifetime with excitation wavelength at 280 nm using pulsed diode light source nano LED with a pulse duration of 1 ns and a repetition rate of 1 MHz. The data were fitted to multiexponential functions after deconvolution of the IRF by an iterative reconvolution technique using IBH DAS 6.2 data analysis software. Analysis of the fluorescence decay data $I(t)$ was done using the following equation

$$I(t) = \sum B_i \exp\left(\frac{-t}{\tau_i}\right) \quad (2)$$

where B_i and τ_i are the pre-exponential factors and the fluorescence lifetime, respectively. The values of χ^2 and residuals serve as the parameters for goodness of the fit. The steady-state and time-resolved fluorescence data were used to construct TRES and TRANES. Fluorescence decay measurement across the emission spectrum (290−410 nm) at particular intervals was used to construct TRES. The fitted fluorescence decays were scaled with steady-state fluorescence intensities.[19,20] The fractional contribution of each component of the fluorescence spectrum at the wavelength of measurement was calculated using the following equation

$$I_i(\lambda) = \frac{\alpha_i \tau_i}{\sum \alpha_i \tau_i} \quad (3)$$

where $I_i(\lambda)$ is the fractional contribution, and α_i and τ_i are the relative amplitude and lifetime of the ith component, respectively. The reconstruction of the time-resolved spectra at different time t was performed using the best fitting parameters as suggested by Maroncelli and Fleming.[21] A JobinYvon Horiba picoseconds-resolved TCSPC spectrometer was further utilized for time-resolved anisotropy decay measurements. The sample was excited at 377 nm using a pulsed diode light source nano LED with a pulse duration of 100 ps and a repetition rate of 1 MHz. Anisotropy $r(t)$ is defined as[22]

$$r(t) = \frac{I_{VV}(t) - GI_{VH}(t)}{I_{VV}(t) + 2GI_{VH}(t)} \quad (4)$$

where I_{VV} and I_{VH} are the emission intensities obtained with the excitation polarizer oriented vertically and emission polarizer oriented vertically and horizontally, respectively. G is the correction term for the relative throughput of each polarization through the emission optics and is given by[23]

$$G = \frac{I_{HV}(t)}{I_{HH}(t)} \quad (5)$$

The entire data analysis was done using IBH DAS 6.2 data analysis software to construct $r(t)$, and from the fitted curve correlation time, τ_r was finally recovered.

Transient Absorption Measurement. Transient absorption spectra were measured using a nanosecond LFP setup (applied photophysics) containing a Nd:YAG (Labseries, Model Lab150, Spectra Physics) laser. The sample was excited at 355 nm (fwhm = 8 ns) laser light. Transients were monitored through absorption of light from a pulsed xenon lamp (150 W).The photomultiplier (R298) output was fed into an Agilent Infiniium oscilloscope (DSO8064A, 600 MHz, 4 Gs/s), and the data were transformed to a computer using the IYONIX software. The software Origin 8.0 was used for curve fitting. The solid curves were obtained by connecting the points using the B-spline option. The samples were deaerated by passing pure argon gas for 20 min prior to each experiment. No degradation of the samples was observed during the experiments.

Molecular Docking. Structural information for bovine beta-lactoglobulin (UniProtKB: LACB_BOVIN) was obtained from Protein Data Bank in Europe (PDBe). Sixty-four structures were found for the full length (sequence range ∼17 to ∼178) protein (Accessed Feb, 2019). All these structures are listed in Table S1. Based on the wwPDB validation report[24−28] on the model quality and the data-fitting quality, the structures were scored on an arbitrary scale of −2 (worst) to 2 (best) (Table S1). The PDB-REDO score[29−31] on the refined geometries of these structures was also obtained and is given in Table S1. Twenty-one structures with the PDB-REDO score of 1.5 or more (Table S1) were obtained from the PDB-REDO repository (pdb-redo.eu; accessed Feb, 2019) for further processing, and finally, the docking was carried out with 17 out of these models. Four structures with missing/duplicate atoms were discarded. Some of these structures contained a native ligand within the binding site. These ligands were removed before the ligand of interest, AD, was

https://dx.doi.org/10.1021/acs.langmuir.9b03506
Langmuir XXXX, XXX, XXX−XXX

docked. Self-docking was not performed. Docking was performed using AutoDock Vina of The Scripps Research Institute,[32] following the previously published protocol.[33] Uniprot residue numbering was used for βLG sequences where two Trp residues are numbered as Trp-35 and Trp-77 instead of Trp-19 and Trp-61, respectively.

RESULTS AND DISCUSSION

CD Spectroscopy. CD spectroscopy is used to detect the alteration in the secondary structure of βLG in the presence of AD. As depicted in Figure 2, the far-UV CD spectrum of βLG

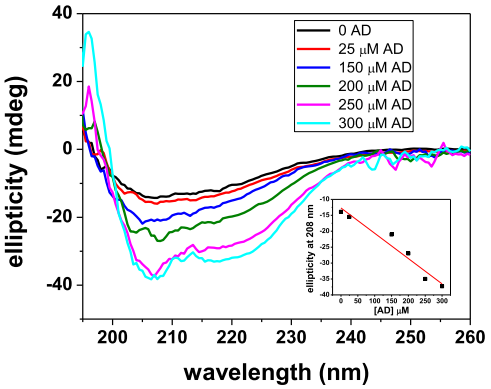

Figure 2. Representative far-UV CD spectra of 70 μM βLG in the absence and presence of various concentrations of AD. The inset shows the change in ellipticity at 208 nm as the function of concentration of AD.

shows a wide negative minimum around 216 nm, which is a signature of β-sheet dominant protein.[34] An interesting observation characteristic of a transition from the β-sheet to α-helix with the development of two minima around 208 and 222 nm is detected on addition of AD to βLG solution. Zhang and Keiderling reported a similar unusual observation while studying the interaction artificial lipid vesicles with βLG.[35] In fact, ellipticity at 208 nm of βLG solution increases linearly with increase in AD concentration as shown in the inset of Figure 2.

UV−vis Absorption Spectroscopy. UV−vis absorption spectroscopy is used to detect the possibility of ground-state interaction between AD and βLG. The absorption spectrum of AD exhibits a maximum around 384 nm in Tris buffer medium. Hyperchromic effect without any spectral shift is observed on gradual addition of βLG to a solution of AD in the Tris buffer as depicted in Figure 3. Such a prominent enhancement in absorbance at 384 nm proves the presence of ground-state interaction between AD and the model protein. In fact, while studying the interaction of aurintricarboxylic acid with serum albumin, Bardhan et al. reported a similar observation of enhancement in absorbance of the drug-like molecule upon addition of BSA and rationalized the observation in the light of formation of a ground-state complex through inclusion of the drug molecule in the protein.[36]

Fluorescence Spectroscopy. Native βLG exhibits intrinsic fluorescence with a maximum around 335 nm, which is mainly attributed to the Trp residues of the protein. As mentioned earlier, βLG has two Trp residues, viz., Trp-19 and Trp-61. It is reported that Trp-19 is in an apolar environment and contributes about 80% of total fluorescence of βLG, while Trp-61 is partly exposed to the aqueous solvent and has minor contribution (about 20%) to the total Trp fluorescence of the protein.[37] Figure 4 and its inset illustrate the progressive

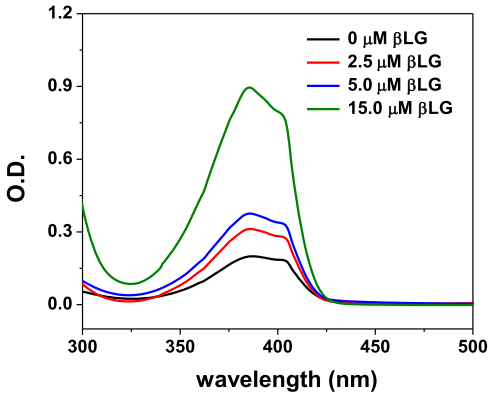

Figure 3. Absorption spectra of 40 μM AD in phosphate buffer showing hyperchromic effect on addition of βLG.

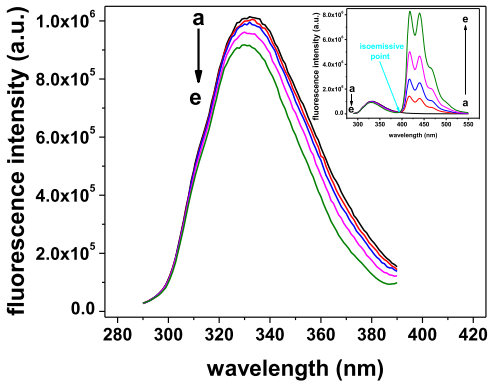

Figure 4. Fluorescence spectra showing the quenching of intrinsic fluorescence of βLG with increase in concentration of AD; λ_{ex} = 280 nm. [βLG] = 10 μM and [AD] = (a) 0, (b) 10, (c) 20, (d) 40, and (e) 80 μM. The inset depicts the same set of spectra in the wavelength region of 290−550 nm, showing the isoemissive point at 393 nm; λ_{ex} = 280 nm.

quenching of intrinsic fluorescence of βLG at 303 K with increase in concentration of AD accompanied by enhancement in fluorescence of the drug and emergence of an isoemissive point at 393 nm. It is interesting to note that λ_{max} of fluorescence spectra of βLG undergoes a slight blue shift with an increase in concentration of AD, indicating that the Trp residues in the protein experience a hydrophobic environment in the presence of AD.

Conventionally, the Stern−Volmer (SV) equation is used to analyze fluorescence quenching data.[38] Figure 5 depicts a linear SV plot for steady-state fluorescence quenching of the protein. In general, a linear SV plot is obtained when the mechanism of fluorescence quenching is either static or dynamic. The existence of static quenching mechanism is evident from the absorption spectroscopic study. To verify the occurrence of dynamic quenching, the time-resolved fluorescence study is carried out, and it is observed that the fluorescence lifetime of βLG at 340 nm is enhanced in the presence of AD (as depicted in Table 1), thus ruling out the possibility of dynamic quenching. For a genuine case of dynamic fluorescence quenching mechanism, the fluorescence lifetime should have been quenched. Hence, it is confirmed that the mechanism of steady-state fluorescence quenching of βLG in the presence of AD is exclusively static in nature. The values of SV constant (K_{SV}) and quenching rate constant (k_q) are determined to be 2.32×10^3 M^{-1} and 8.32×10^{11} M^{-1} s^{-1}, respectively, at 303

https://dx.doi.org/10.1021/acs.langmuir.9b03506
Langmuir XXXX, XXX, XXX−XXX

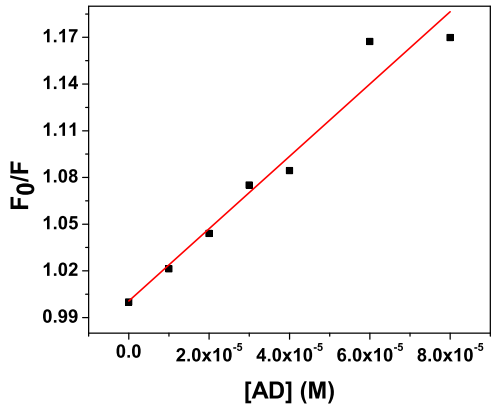

Figure 5. SV plot for quenching of steady-state fluorescence of βLG by AD; [βLG] = 10 μM and [AD] ranges from 0 to 80 μM.

Table 1. Variation in the Nanosecond-Resolved Fluorescence Lifetime of βLG ($\langle\tau\rangle$) with an Increase in the Concentration of AD[a]

[AD] μM	A_1	τ_1 (ns)	A_2	τ_2 (ns)	$\langle\tau\rangle^b$ (ns)	χ^2
0	67.68	1.08	32.32	3.81	2.79	1.13
25	69.01	1.12	30.99	4.14	3.00	1.14
50	73.19	1.26	26.81	4.52	3.11	1.03
100	79.21	1.43	27.09	5.00	3.37	1.13

[a] λ_{ex} = 280 nm and λ_{em} = 340 nm; [βLG] = 8 μM. [b] $\langle\tau\rangle = \frac{A_1\tau_1^2 + A_2\tau_2^2}{A_1\tau_1 + A_2\tau_2}$.

K. A confirmatory proof of aforementioned static mechanism of quenching is obtained from the temperature dependence of the K_{SV} values. The value of K_{SV} is found to decrease with increase in temperature as shown in Table 2, suggesting the

Table 2. Variation of K_{SV} and k_q Values with Temperature for the Interaction of AD with βLG

temperature (K)	K_{SV} (M^{-1})	k_q (M^{-1} s^{-1})	R^2
298	3.33×10^3	1.19×10^{12}	0.9622
303	2.32×10^3	8.32×10^{11}	0.9487
308	1.95×10^3	7.00×10^{11}	0.9460

static nature of quenching. It may be mentioned here that in both AD−HSA and AD−BSA systems, simultaneous static and dynamic mechanism of quenching of intrinsic fluorescence of the protein by AD is observed.

It is to be noted that the value of k_q in the present case is higher than the upper limit of the value of k_q for a diffusion-controlled process, which is of the order of 10^{10}, implying the prevalence of static quenching mechanism. Sometimes, another common photoinduced process, which is often invoked to account for such high value of k_q, is Förster resonance energy transfer (FRET) from the photoexcited Trp moiety of the protein to the drug molecules (as in AD−HSA and AD−BSA systems). The authentic proof of occurrence of FRET is the reduction in lifetime of the donor in the presence of the acceptor moiety.[39,40] However, in the present case, the possibility of FRET is overruled because the fluorescence lifetime of Trp is enhanced in the presence of AD (as depicted in Table 1).

Table 1 shows that native βLG shows biexponential fluorescence decay, which is consistent with previous literature reports.[34]

Portugal and co-workers reported the "unquenching" of fluorescence decay times of βLG in the presence of acrylamide.[41] In fact, they suggested that although steady-state fluorescence of βLG accounts for the contributions of both Trp-19 and 61, fluorescence decay of the said protein accounts exclusively for the lifetime of Trp-19. Thus, in the present case, increase in fluorescence lifetime of βLG in the presence of AD implies that this acridine derivative directly perturbs the immediate vicinity of Trp-19 residue. Tryptophan can undergo sub-nanosecond timescale rotational motions, even when located in the hydrophobic core of proteins.[41] Portugal et al. suggested that alteration in Trp-19 mobility gives rise to a number of rotamers, and this proposition was later discussed by Harvey et al.[41,42] They further suggested simultaneous change in amplitude and decay time components of Trp-19 fluorescence, indicating the alteration of Trp-19 mobility on binding with any external molecule. In the present case, it has been clearly noted that both the amplitude and the lifetime of the Trp fluorescence alter with gradual addition of AD (as shown in Table 1). Therefore, it may be inferred in the present case, as per Portugal's proposition, the interconversion between the rotamers is fast enough to compete with the excited-state deactivation. According to Portugal, if the interconversion between the rotamers is too slow to compete with excited-state deactivation, then any external factor (addition of AD in the present case) that affects the interconversion rate will be reflected only in the pre-exponential factors, and the decay times will remain constant.[41] A detailed analysis of fluorescence lifetime of βLG on binding with AD as displayed in Table 1 shows that: (i) the increase in both decay times (τ_1 and τ_2) associated with Trp-19 along with (ii) the increase in amplitude associated with the shorter decay time (A_1) at the expense of the amplitude associated with the longer decay time (A_2). The plausible explanation of these observations is decrease in rate constant for the interconversion between quenched and unquenched conformers of Trp-19, which may arise from decrease in mobility of Trp-19 on binding with AD.

Steady-state and time-resolved fluorescence spectra are utilized to construct TRES and TRANES. Koti and Periasamy suggested that being a model-free method, TRANES is a more convenient method of analysis of wavelength-dependent fluorescence decay compared to TRES.[19] TRANES analysis primarily helps to determine the number of emissive species present in the system. Figure 6 shows the TRANES profile of a solution containing both βLG and AD using λ_{ex} = 280 nm,

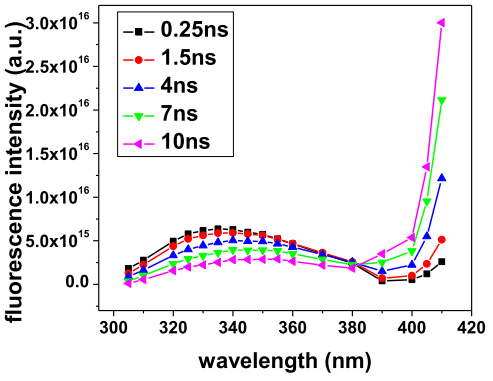

Figure 6. TRANES of βLG (10 μM) in the presence of AD (8 μM) in Tris-HCl buffer solution between time 0.25−10 ns; λ_{ex} = 280 nm.

https://dx.doi.org/10.1021/acs.langmuir.9b03506
Langmuir XXXX, XXX, XXX−XXX

depicting only one isoemissive point at 380 nm. The presence of a single isoemissive point indicates the existence of two species in the excited state, viz., free βLG and βLG bound to AD. While studying the interaction of AD with HSA, a protein with a sole Trp residue, we have observed a single isoemissive point in the TRANES,[15] implying the involvement of a single Trp in interaction with AD; however, while studying the interaction of AD with BSA,[16] a protein with two Trp residues in varied environments, we have reported that TRANES contained two isoemissive points emerging at different time intervals, which is rationalized in the light of involvement of both the Trp residues of BSA in interaction with AD. In the present case, owing to the emergence of a single isoemissive point in the TRANES, it seems that only one Trp residue of βLG directly interacts with the acridine derivative, inspite of the fact that βLG contains two Trp residues in varied environments and as inferred from the time-resolved fluorescence study, the interacting Trp residue is possibly Trp-19.

Time-resolved anisotropy measurement is helpful in providing information about rotational motion and/or rotational relaxation of a fluorophore in a rigid environment.[23] The anisotropy decay profiles of AD in buffer solution and in the protein environment are depicted in Figure 7A,B, respectively.

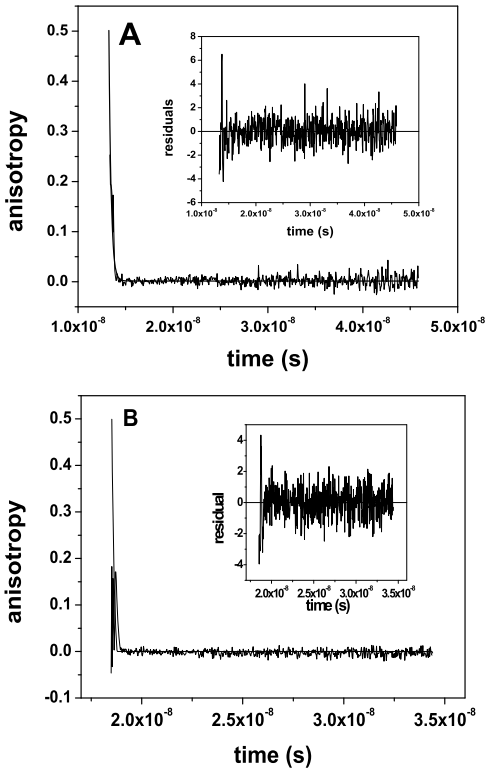

Figure 7. Time-resolved anisotropy decay curves for (A) a solution of 8 μM AD and (B) a solution containing 8 μM AD + 10 μM βLG; λ_{ex} = 377 nm and λ_{em} = 420 nm.

For a solution containing only AD in buffer solution, the anisotropy decay fits to a single exponential function, and the value of rotational correlation time is found to be 0.235 ns, whereas, for a solution containing AD in βLG, the anisotropy appears to be bi-exponential with two correlation times—a shorter component of 0.132 ns (38.34%) and a longer component of 26.6 ns (61.66%). The functional form of the biexponential anisotropy decay is given by the following relation

$$r(t) = r_0 \times \left[\alpha_{1r} \exp\left(-\frac{t}{\tau_{1r}}\right) + \alpha_{2r} \exp\left(-\frac{t}{\tau_{2r}}\right)\right] \quad (6)$$

where r_0 is the limiting anisotropy that describes the inherent depolarization of the fluorophore, and α_{ir} is the pre-exponential factor that provides the fraction of the ith rotational time, that is, τ_{ir}. The emergence of two components of correlation times obtained from the bi-exponential pattern of anisotropy decay of AD in the presence of βLG indicates the presence of two dynamic processes occurring on different time scales. The value of average correlation time (as shown in Table 3) apparently indicates that AD experiences a constrained environment in the presence of the protein. Average correlation time is calculated using the following equation

$$\langle\tau_r\rangle = \alpha_{1r}\tau_{1r} + \alpha_{2r}\tau_{2r} \quad (7)$$

Here, α_{1r} and α_{2r} are the magnitudes of the faster and slower components, respectively, whereas τ_{1r} and τ_{2r} are the observed fast and slow components of the anisotropy decay, respectively.

The origin of the biexponential behavior of the dye in the protein environment may be rationalized in the light of numerous reasons. First, the short and long components of anisotropy decay of AD in the presence of βLG can be assigned to free AD and protein-bound AD, respectively. However, owing to the moderately high value of binding constant of the ligand with the protein (as discussed later in this section), the basis of such a proposition may be questioned. Second, the biexponential nature may arise because of the rotational diffusion of AD bound to two different regions of the protein having distinctly different environments (hydrophilic and hydrophobic interaction sites of βLG). This proposition may also be questioned because the experimental findings as well as docking study suggest that AD is interacting with the hydrophobic pocket of the protein-bearing Trp-19 and is thus not distributed to more than one region of the proteins having diverse microenvironments. Third, it may arise because of different species originating from varied modes of binding of AD to various rotamers of Trp-19. Although the rotamers of Trp-19 are present in the hydrophobic pocket, the rotation of Trp residue may create a situation where it can facilitate the formation of hydrogen bond with AD. This type of hydrogen bonded species may be responsible for lower rotation time while the species, which is hydrophobically bonded, is assigned higher rotational time. Finally, in tune with a number of literature reports, the observed biexponential anisotropy decay of AD in the protein

Table 3. Rotational Parameters of AD in the Aqueous Buffer Phase and in the Presence of βLG

environment	τ_{ir} (ns)	τ_{2r} (ns)	α_{1r} (%)	α_{2r} (%)	$\langle\tau_r\rangle$ (ns)	S	θ (deg)	τ_W (ns)	$D_W \times 10^{-8}$ (s^{-1})
aq buffer	0.235		100		0.235				
βLG	0.132	26.6	38.34	61.66	16.45	0.785	31.89	0.139	5.92

https://dx.doi.org/10.1021/acs.langmuir.9b03506
Langmuir XXXX, XXX, XXX−XXX

Table 4. Values of Binding and Thermodynamic Parameters for the AD−βLG System at Different Temperatures

temperature (K)	n	K (M^{-1})	ΔG° (kJ mol^{-1})	ΔH° (kJ mol^{-1})	ΔS° (J mol^{-1} K^{-1})
298	1.06	6.17×10^3	−22.04	−151.96	−435.98
303	1.05	3.76×10^3	−19.86		
308	0.90	0.84×10^3	−17.68		

environment can be explained in terms of "wobbling-in-cone" model,[43−47] which suggests that such bi-exponential decay may be interpreted in terms of occurrence of different kinds of rotational motions of the probe in the protein environment. According to this model, the fluorescence anisotropy decay is a product of three independent motions:

(i) wobbling of the probe $r_W(t)$ with a time constant τ_W,
(ii) translation of the probe $r_D(t)$, along the surface of the protein, with a time constant τ_D, and
(iii) overall rotation $r_P(t)$ of the protein with a time constant τ_P.

Thus, $r(t)$ may be decomposed as a product of three independent motions as

$$r(t) = r_W(t) r_D(t) r_P(t) \tag{8}$$

Again, $r(t)$ maybe expressed in terms of the generalized order parameter S as

$$r(t) = r_0\left[S^2 + (1 - S^2)\exp\left(-\frac{t}{\tau_W}\right)\right]\exp\left[-t\left(\frac{1}{\tau_D} + \frac{1}{\tau_P}\right)\right] \tag{9}$$

In the wobbling-in-cone model, S is related to the semi-cone angle θ as follows[44]

$$S = 0.5 \cos\theta(1 + \cos\theta) \tag{10}$$

The order parameter S is a measure of the spatial restriction having values between 0 (corresponding to unrestricted motion) to 1 (for complete restriction on the motion). Comparing eqs 8 and 9, the following relations are obtained

$$S^2 = \alpha_{2r} \tag{11}$$

$$\frac{1}{\tau_{2r}} = \frac{1}{\tau_D} + \frac{1}{\tau_P} \tag{12}$$

$$\frac{1}{\tau_{1r}} = \frac{1}{\tau_W} + \frac{1}{\tau_{2r}} \tag{13}$$

The wobbling-in-cone diffusion co-efficient D_W is given by the following equation for $\theta \leq 30^\circ$

$$D_W = \frac{7\theta^2}{24\tau_W} \tag{14}$$

whereas for $\theta \geq 30^\circ$, D_W is represented as follows

$$D_W = \{(1 - S^2)\tau_W\}^{-1}\left[\frac{x^2(1+x)^2}{2(x-1)}\left\{\ln\left(\frac{1+x}{2}\right) + \left(\frac{1-x}{2}\right)\right\} + \left(\frac{1-x}{24}\right)(6 + 8x - x^2 - 12x^3 - 7x^4)\right] \tag{15}$$

where $x = \cos\theta$.

Equation 15 has been used to calculate the value of D_W as $\theta > 30^\circ$ in the present case. The calculated parameters associated with the wobbling motion of the drug within the protein are compiled in Table 3.

A quantitative assessment for the drug−protein binding interaction can be expressed in terms of evaluation of binding constant (K), and binding site number (n) based on analysis of fluorescence quenching data can be obtained using the following equation[48]

$$\log\left(\frac{F_0 - F}{F}\right) = \log K + n \log[Q] \tag{16}$$

where F_0 and F are the fluorescence intensities in the absence and presence of quencher, and $[Q]$ is the concentration of quencher. From the intercepts and slopes of the plot of $\log(F_0 - F)/F$ versus $\log[Q]$ at various temperatures (as depicted in Figure S1), the values of K and n are obtained. Further, the fluorescence quenching study at various experimental temperatures helps in evaluating the thermodynamic parameters such as ΔG°, ΔH°, and ΔS° associated with AD−βLG interaction. Assuming that the value of ΔH° remains almost unaltered within the range of experimental temperature, the thermodynamic parameters can be evaluated using van't Hoff and Gibbs−Helmholtz equations.

$$\ln K = -\left(\frac{\Delta H^\circ}{RT}\right) + \left(\frac{\Delta S^\circ}{R}\right) \tag{17}$$

and

$$\Delta G^\circ = \Delta H^\circ - T\Delta S^\circ \tag{18}$$

The values of ΔH° and ΔS° are obtained, respectively, from the slope and intercept of the plot of ln K versus $1/T$. ΔG° at different temperatures using eq 18. Table 4 summarizes the values of binding and thermodynamic parameters at various temperatures using the results obtained from the analysis of fluorescence quenching data. As binding constants and thermodynamic parameters are evaluated by the temperature-dependent fluorescence study, it is pertinent to mention here that with increase in temperature, there is progressive quenching in the intrinsic fluoresce of βLG (as depicted in Figure S2). However, because we deal with the relative change in fluorescence intensity, the change in protein fluorescence with temperature does not hamper the measurement of binding and thermodynamic parameters.

The values of K as depicted in Table 4 are comparable with those obtained for interactions of βLG with chloramphenicol[34] and norfloxacin.[49] The signs of the thermodynamic parameters are often used to find out the principal binding forces involved in drug−protein interaction. The model of interaction on the basis of thermodynamic parameters as suggested by Ross and Subramanian is as follows:[50]

(i) $\Delta H > 0$ and $\Delta S > 0$ correspond to hydrophobic forces
(ii) $\Delta H < 0$ and $\Delta S < 0$ correspond to van der Waals interaction and hydrogen bond formation

https://dx.doi.org/10.1021/acs.langmuir.9b03506
Langmuir XXXX, XXX, XXX−XXX

(iii) $\Delta H < 0$ and $\Delta S > 0$ correspond to the electrostatic interaction

Table 4 suggests the exothermicity of the reaction ($\Delta H°$ is negative) with an overall negative Gibb's free energy change, indicating the spontaneity of AD−βLG interaction. It is observed that the value of K decreases with rise in temperature, implying the formation of a complex between AD and βLG, which gradually loses its stability at higher temperature, substantiating the occurrence of static mechanism of fluorescence quenching. Further, negative values of $\Delta H°$ and $\Delta S°$ suggest the predominance of van der Waals interaction and hydrogen bonding in the binding interaction.

Docking Study. Protein Data Bank (PDB) contains numerous entries of βLG, however, according to the wwPDB validation report, most of the structures are not fit for use in further study. The model quality score as well as the electron density map fitting score are given in Table S1. Therefore, we sought the PDB-REDO scores of these entries, which are derived after further refinement and fitting of these structures. Finally, we have obtained all the best quality crystal structures of bovine βLG (Table 5 and S1) having a redo score of 1.5 or more (arbitrary scale; vide methods) from PDB-REDO repository for molecular docking simulation. Figure 8 illustrates a comparison of AD docking with other known ligands.

Table 5. Binding Energies and Binding Site of AD on βLG

PDB ID	E (kJ/mol)	binding site
1BEB	−31.7984	ex situ
1BSO	−24.2672	ex situ
1YUP	−25.104	ex situ
1BSQ	−24.6856	ex situ
1BSY	−32.6352	in situ
2BLG	−23.012	ex situ
2GJ5	−31.7984	in situ
2Q39	−24.2672	ex situ
3NQ3	−28.8696	ex situ
3UEU	−34.3088	in situ
3UEV	−34.3088	in situ
4IB7	−25.5224	ex situ
4IB8	−26.7776	ex situ
4IBA	−35.1456	in situ
4Y0Q	−33.0536	in situ
4Y0R	−31.38	in situ
6FXB	−26.7776	ex situ

It is evident from the docking results that AD preferentially binds into the known ligand binding cavity of βLG. However, Figure 8B shows some other energetically favorable ectopic binding sites of AD on βLG. These ectopic binding sites are more exposed to the water and contained polar amino acid residues, which can form hydrogen bonding interactions with AD.

Docking suggested that AD binds to the known (SDS or long chain fatty acid) binding site of the protein. Average binding energy for in situ binding was found to be −33.23 ± 0.57 kJ/mol. βLG is a beta barrel protein containing a barrel-shaped ligand binding site made of eight antiparallel beta strands. As discussed earlier in the Introduction, the inner residues of this beta-barrel form the pharmacophore for ligand binding. The best binding pose of AD as obtained by molecular docking is shown in Figure 9 (same as Figure 8C). AD is found to go inside the beta-barrel of βLG. Distances and the relative positions of the two tryptophan residues from the bound AD are also shown in Figure 9. Trp-35, which is positioned inside the barrel, was found to be about 10 Å away from the AD while the solvent-exposed tryptophan (Trp-77) is around 19 Å away. The interacting residues, which also form the inner lining of the barrel, are shown in Figure 10. Inner lining of this barrel is found to be completely hydrophobic in nature. Apart from the hydrophobic interactions, there is a phenylalanine inside the barrel that forms pi-stacking with the AD.

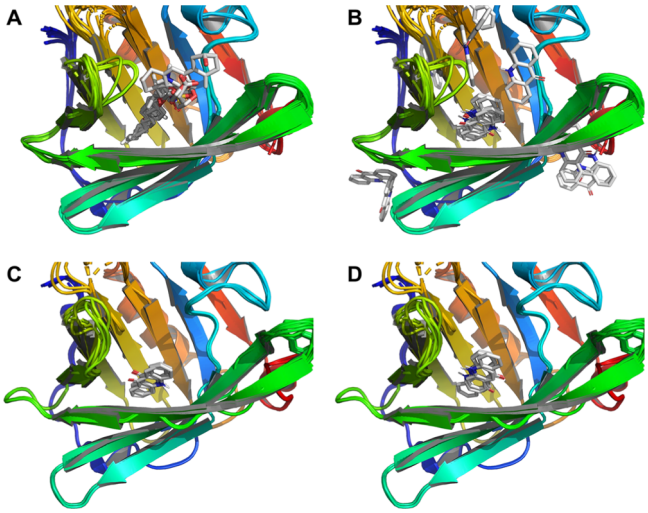

Figure 8. Comparison of AD docking with other known ligands. (A) Superposition of all the ligand-bound crystal structures (as listed in Table S1) of βLG. (B) Superposition of all the best docked conformations of AD as listed in Table 5. (C,D) Two possible orientations of AD in the binding cavity of βLG as obtained by docking.

Although the inner lining of the βLG binding site cavity is formed by hydrophobic residues, a polar amino acid Gln120 remains obscured by two neighboring amino acids Leu119 and Phe121 inside the binding cavity. Figure 11 shows the orientation of the Gln120 side chain and its distance from AD. This residue is capable of forming hydrogen bond with both the lowest energy conformers of AD as shown in Figure 8C,D, under solvated and dynamic condition. Proximity of Phe 121 suggests that it may also form Sutor-type hydrogen bonding with AD, which is presently out of the scope of docking and MD simulation.

Solvent-accessible surface area, which is abbreviated as SASA, is a measure of forming contacts between the atoms on the surface of a protein and the solvent (water) molecules. Although molecular docking does not directly give the solvent effects in ligand protein interactions, the effect of solvent exclusion can be derived from the docking experiments by probing the changes in the SASA of protein residues and the ligand. Changes in the accessible surface area of the interacting residue are shown in Figure 12. Val57, Leu62, Ile72, Ile87, Val108, Phe121, and Met123 are the residues that show maximum reduction in solvent accessible surface area upon AD binding as shown in Figure 12. Further, the SASA of AD is found to be reduced to 12.68 Å^2 from 336.79 Å^2 as obtained from the computation of SASA in the docked complex. Therefore, when AD enters into the binding cavity of the protein, it gets completely solvent excluded (∼96% reduction

https://dx.doi.org/10.1021/acs.langmuir.9b03506
Langmuir XXXX, XXX, XXX−XXX

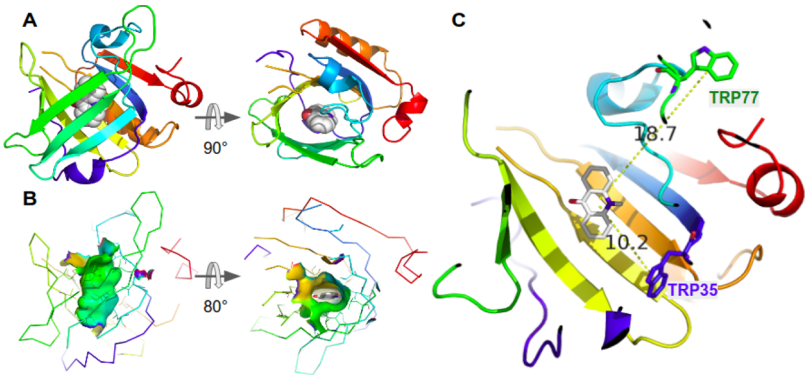

Figure 9. Best binding mode of AD with βLG as obtained by molecular docking simulation. (A) Cartoon representation of βLG (PDB ID: 4IBA) bound with AD (CPK model). N to C terminal of βLG is colored in rainbow. (B) Surface view of the binding site cavity. (C) Slice view *XZ* plane showing the relative positions of the two Trp in βLG with respect to the bound AD. Distances are given in Å.

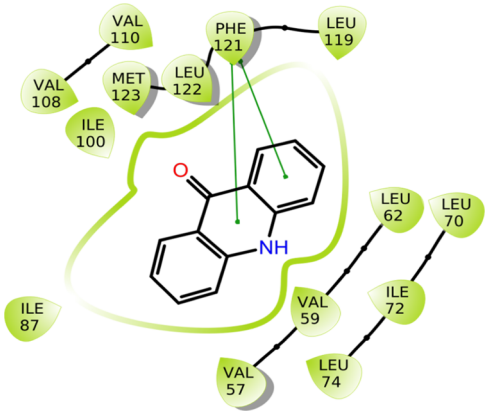

Figure 10. Interaction diagram of AD with bovine βLG (PDB ID: 4IBA). Hydrophobic residues are shown in green. The green straight line connecting AD and Phe121 indicates pi-stacking interaction.

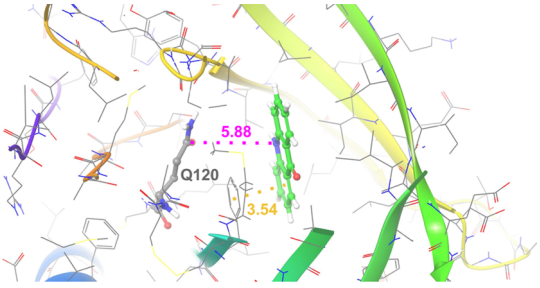

Figure 11. Orientation of Gln120 side chain and its distance from AD. Orientation and distance of Phe 121 are also shown.

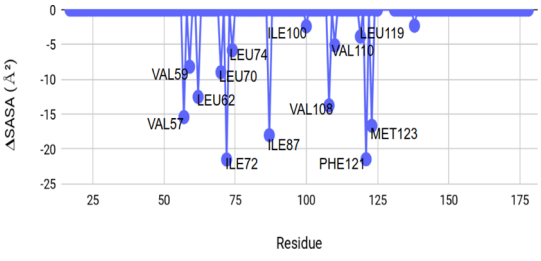

Figure 12. Changes in the accessible surface area of the interacting residues of bovine βLG (PDB ID: 4IBA) as obtained by molecular docking simulation.

in SASA), suggesting that entropy of solvent exclusion/reorganization also plays an important role in AD−βLG binding.

Laser Flash Photolysis. Figure 13A,B traces the transient absorption spectra of 20 μM AD at 0.65, 0.96, 1.36, 1.96, 2.96, and 4.96 μs time delays after the triggering of the laser pulse in the absence and presence of βLG, respectively. Figure 13A shows that the spectral signatures of ^{3}AD* at 360 and 420 nm are quite stable at longer time delay. On comparing Figure 13A,B, it is evident that the spectral features of ^{3}AD* undergo a noticeable change on addition of βLG. Literature reports suggest that the transient absorption spectral signature of Trp$^\bullet$ is at 510 nm.[51−53] Further, we have already reported that the triplet−triplet transient absorption spectrum of AD has a broad peak in the wavelength region spanning from 400 to about 500 nm with a maximum at 430 nm along with a small peak around 350 nm.[54] Figure 13C shows that on adding βLG to a solution of AD, there is an overall increase in absorbance in the wavelength region around 360, 420, and 470 nm. Das and Nath reported that during interaction of thioxanthone with tryptophan,[55] there is formation of a broad band at 460−520 nm, which they assigned to Trp$^\bullet$, although the characteristic peak of the amino acid radical is known to appear around 510 nm. From time-resolved fluorescence studies, it has been observed that the TRANES profile depicts only one isoemissive point, inferring the existence of equilibrium between free βLG and βLG bound to AD in the excited state. The formation of a complex between βLG and AD in the ground state has already been confirmed from steady-state absorption studies and also the fluorescence quenching is found to be static in nature. Therefore, the overall increase in the absorbance in the LFP study may be because of the complex between βLG and AD that is initially formed in the ground state and subsequently excited to the triplet state through the corresponding singlet state. It has also been observed that AD interacts with the Trp-19, which is 10 Å apart, in the hydrophobic region. Moreover the phenylalanine inside the beta-barrel forms pi-stacking with the AD. Thus, AD remains within a confined environment of the protein. Previously, we had reported that a model antitumor quinone drug, menadione (MQ) undergoes PET with 2′-deoxyadenosine (ADS) studied in the homogeneous polar organic solvent; however, it primarily undergoes hydrogen abstraction in heterogeneous micellar medium because of their confinement within the hydrophobic region of micelles, which facilitates hydrogen bonding between the carbonyl group of MQ and

https://dx.doi.org/10.1021/acs.langmuir.9b03506
Langmuir XXXX, XXX, XXX−XXX

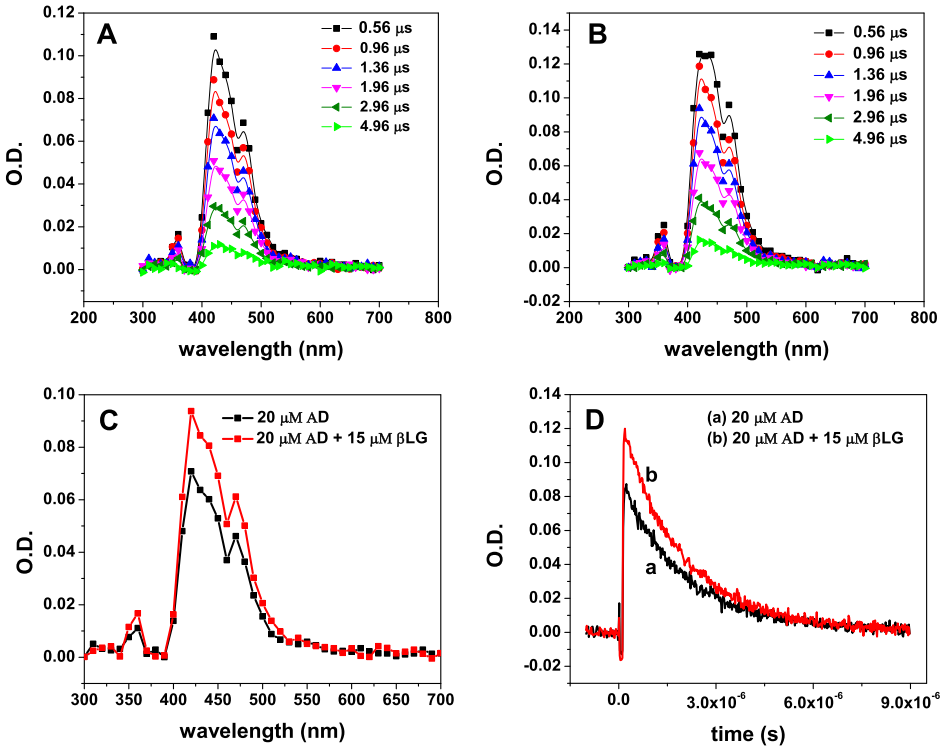

Figure 13. (A): Time-resolved transient absorption spectra of 20 μM AD at 0.56 (■), 0.96 (●), 1.36 (▲), 1.96 (▼), 2.96 (◀), and 4.96 (▶) μs after the laser flash at 355 nm. (B) Time-resolved transient absorption spectra of 20 μM AD in the presence of 15 μM βLG at 0.56 (■), 0.96 (●), 1.36 (▲), 1.96 (▼), 2.96 (◀), and 4.96 (▶) μs after the laser flash at 355 nm. (C) Transient spectra of (a) 20 μM AD (black ■) and (b) 20 μM AD in the presence of 15 μM βLG (red ■) in Tris-HCl buffer of pH 7.4 at 1.36 μs after the laser flash at 355 nm. (D) Decay profiles of (a) 20 μM AD and (b) 20 μM AD in the presence of 15 μM βLG in Tris-HCl buffer of pH 7.4 at 470 nm after laser flash at 355 nm.

amino group of ADS.[56] This also may happen between the carbonyl group of AD and a favorable rotamer of Trp-19 of the protein that facilitates the formation of the complex through hydrogen bonding. However, because of mobility of Trp-19 forming different rotamers, the stability of the complex gets reduced. In fact, excited-state hydrogen bonding is common phenomenon and is of immense interest to the researchers.[57] Nonetheless, stability of the complex would be more in the excited state where electron delocalization within AD is more compared to its ground state. This leads to the dissociation of the complex; however, for some of the rotamers, it may be through hydrogen abstraction, enhancing the formation of $Trp^{\bullet}$ and $ADH^{\bullet}$. Thus, increase in absorbance in the wavelength region of 470−510 nm may originate from $Trp^{\bullet}$ and that at 360 and 420 nm may be possibly assigned to formation of $ADH^{\bullet}$. The LFP study thus proves that the inference drawn regarding the nature of binding force, especially the involvement of hydrogen bonding, from fluorescence study at various temperatures is valid.

An ambiguity arises regarding the amino acid residue of the protein taking part in hydrogen bonding, derived from the results of spectroscopy and docking studies. The initial hint of involvement of hydrogen bonding is obtained from the fluorescence study under varied temperatures, which gives an indication regarding the nature of interacting forces. Also, a clue regarding the participation of Trp-19 in hydrogen bonding is derived from the time-resolved fluorescence anisotropy study. Docked conformations suggest that Gln 120 or Phe 121 may possibly be involved in hydrogen bonding. It is pertinent to point out that the docking study takes the entire system into consideration in contrast to the fluorimetric approach, which probes the immediate microenvironment in and around the fluorophore. Docking involves the attainment of optimized structure as well as the orientations of the drug and the protein molecules so that the total free energy of the whole system is minimized. Thus, minimum energy conformation is given more significance in this case, although the involvement of other conformations is also feasible. This may give rise to disagreement between the experimental and docking results, and such disagreements were reported previously.[18] It may be proposed that owing to the dynamic nature of the protein structure of βLG, AD, which is housed inside the hydrophobic cavity of the protein, comes in the vicinity of Trp-19, and the keto functional group of the acridine derivative helps in the formation of hydrogen bonding in the photoexcited state of the protein. The electronic distribution and orientation of the atoms of the amino acid residues may completely differ in the photoexcited state compared to that in the ground state. In fact, we have already discussed that the time-resolved fluorescence study suggests the possibility of involvement of number of rotamers of Trp-19 in binding with AD, which may help in the formation of hydrogen bonds. However, such a possibility of formation of rotamers of Trp is not considered during docking analysis. Results obtained using the LFP technique supports the involvement of Trp-19 in hydrogen bonding, as suggested by the fluorescence spectroscopic study.

■ CONCLUSIONS

The present article primarily focuses on the mode of binding of AD with βLG. It is found that AD possibly binds to the hydrophobic pocket of βLG which houses Trp-19. Integration of our previous reports[15,16] with the present results indicates

https://dx.doi.org/10.1021/acs.langmuir.9b03506
Langmuir XXXX, XXX, XXX−XXX

that the prime difference between the interaction of AD with serum albumins and βLG is that PET and FRET are the key phenomena involved in the interaction of AD with serum albumins, while hydrogen abstraction assisted by hydrogen bonding is prevalent in the case of interaction of AD with βLG. Both PET and hydrogen abstraction assisted by hydrogen bonding are confirmed using LFP technique. In fact, the manifestation of PET in AD−BSA and AD−HSA systems is exhibited by quenching of fluorescence lifetime of the serum albumins in the presence of AD. On the contrary, in the AD−βLG system, fluorescence lifetime of the protein is enhanced in the presence of AD, which gives an indication of the involvement of rotamers of Trp. The possibility of FRET is overruled in the AD−βLG system because of increase in fluorescence lifetime of Trp in the presence of AD. Moreover, in case of AD−BSA and AD−HSA systems, the mechanism of quenching of steady-state fluorescence of the proteins by AD is simultaneously static and dynamic, while in case of AD−βLG system, the nature of mechanism is exclusively static. The contribution of dynamic quenching accounts for the diffusion-controlled process in the system, may be related to PET for AD−BSA and AD−HSA systems, which is completely absent in the case of AD−βLG system. Finally, we feel that the extension of this work to study the interaction of AD with allied proteins/enzymes can possibly help in exploring and establishing its biological significance.

■ ASSOCIATED CONTENT

Supporting Information

The Supporting Information is available free of charge at https://pubs.acs.org/doi/10.1021/acs.langmuir.9b03506.

Available models of BLG in PDBe and PDB Redo databases and their quality, according to wwPDB validation report, plots of $\log(F_0 - F)/F$ versus $\log[Q]$ at 298, 303, and 308 K, and progressive quenching of intrinsic fluorescence of 10 μM βLG with rise in temperature (PDF)

■ AUTHOR INFORMATION

Corresponding Author

Brotati Chakraborty − *Department of Chemistry, Bejoy Narayan Mahavidyalaya, Itachuna, West Bengal 712147, India;* orcid.org/0000-0002-0558-1620; Email: brotati07@gmail.com

Authors

Chaitrali Sengupta − *S.N. Bose National Centre for Basic Sciences, Kolkata, West Bengal 700106, India*

Uttam Pal − *S.N. Bose National Centre for Basic Sciences, Kolkata, West Bengal 700106, India*

Samita Basu − *Chemical Sciences Division, Saha Institute of Nuclear Physics, Kolkata 700064, India;* orcid.org/0000-0003-1629-2979

Complete contact information is available at: https://pubs.acs.org/10.1021/acs.langmuir.9b03506

Notes

The authors declare no competing financial interest.

■ ACKNOWLEDGMENTS

Financial help from the Biomolecular Assembly, Recognition and Dynamics (BARD) project of Saha Institute of Nuclear Physics, Department of Atomic Energy, Government of India is greatly acknowledged. The authors are thankful to Dr. Soma Mondal, Saha Institute of Nuclear Physics, Kolkata, for her help.

■ REFERENCES

(1) Teng, Z.; Xu, R.; Wang, Q. Beta-lactoglobulin-based encapsulating systems as emerging bioavailability enhancers for nutraceuticals: a review. *RSC Adv.* **2015**, *5*, 35138−35154.

(2) Cho, Y.; Batt, C. A.; Sawyer, L. Probing the retinol-binding site of bovine beta-lactoglobulin. *J. Biol. Chem.* **1994**, *269*, 11102−11107.

(3) Kontopidis, G.; Holt, C.; Sawyer, L. The ligand-binding site of bovine β-lactoglobulin: evidence for a function? *J. Mol. Biol.* **2002**, *318*, 1043−1055.

(4) Narayan, M.; Berliner, L. J. Mapping fatty acid binding to β-lactoglobulin: ligand binding is restricted by modification of Cys 121. *Protein Sci.* **1998**, *7*, 150−157.

(5) Wang, Q.; Allen, J. C.; Swaisgood, H. E. Binding of vitamin D and cholesterol to β-lactoglobulin. *J. Dairy Sci.* **1997**, *80*, 1054−1059.

(6) Hasni, I.; Bourassa, P.; Tajmir-Riahi, H.-A. Binding of cationic lipids to milk β-lactoglobulin. *J. Phys. Chem. B* **2011**, *115*, 6683−6690.

(7) Armstrong, R. W.; Kurucsev, T.; Strauss, U. P. Interaction between acridine dyes and deoxyribonucleic acid. *J. Am. Chem. Soc.* **1970**, *92*, 3174−3181.

(8) Higashi, N.; Takahashi, M.; Niwa, M. Immobilization of DNA through intercalation at self-assembled monolayers on gold. *Langmuir* **1999**, *15*, 111−115.

(9) Read, M.; Harrison, R. J.; Romagnoli, B.; Tanious, F. A.; Gowan, S. H.; Reszka, A. P.; Wilson, W. D.; Kelland, L. R.; Neidle, S. Structure-based design of selective and potent G quadruplex-mediated telomerase inhibitors. *Proc. Natl. Acad. Sci. U. S. A.* **2001**, *98*, 4844−4849.

(10) Baruah, H.; Day, C. S.; Wright, M. W.; Bierbach, U. Metal−Intercalator-Mediated Self-Association and One-Dimensional Aggregation in the Structure of the Excised Major DNA Adduct of a Platinum− Acridine Agent. *J. Am. Chem. Soc.* **2004**, *126*, 4492−4493.

(11) Campbell, N. H.; Parkinson, G. N.; Reszka, A. P.; Neidle, S. Structural basis of DNA quadruplex recognition by an acridine drug. *J. Am. Chem. Soc.* **2008**, *130*, 6722−6724.

(12) Fritsch, C.; Goerz, G.; Ruzicka, T. Photodynamic therapy in dermatology. *Arch. Dermatol.* **1998**, *134*, 207−214.

(13) Varnell, E. D.; Kaufman, H. E. Photodynamic inactivation with proflavine: quantitative comparison with iodo-deoxyuridine. *Infect. Immun.* **1973**, *7*, 518−519.

(14) Satonaka, H.; Kusuzaki, K.; Matsubara, T.; Shintani, K.; Wakabayashi, T.; Nakamura, T.; Matsumine, A.; Uchida, A. Flash wave light strongly enhanced the cytocidal effect of photodynamic therapy with acridine orange on a mouse osteosarcoma cell line. *Anticancer Res.* **2007**, *27*, 3339.

(15) Chakraborty, B.; Mitra, P.; Basu, S. Spectroscopic exploration of drug-protein interaction: a study highlighting the dependence of the magnetic field effect on inter-radical separation distance formed during photoinduced electron transfer. *RSC Adv.* **2015**, *5*, 81533−81545.

(16) Chakraborty, B.; Sengupta, C.; Pal, U.; Basu, S. Acridone in a biological nanocavity: detailed spectroscopic and docking analyses of probing both the tryptophan residues of bovine serum albumin. *New J. Chem.* **2017**, *41*, 12520.

(17) Martins, P. A. T.; Gomes, F.; Vaz, W. L. C.; Moreno, M. J. Binding of phospholipids to β-Lactoglobulin and their transfer to lipid bilayers. *Biochim. Biophys. Acta* **2008**, *1778*, 1308−1315.

(18) Chakraborty, B.; Roy, A. S.; Dasgupta, S.; Basu, S. Magnetic field effect corroborated with docking study to explore photoinduced electron transfer in drug− protein interaction. *J. Phys. Chem. A* **2010**, *114*, 13313−13325.

(19) Koti, A. S. R.; Krishna, M. M. G.; Periasamy, N. Time-resolved area-normalized emission spectroscopy (TRANES): A novel method

for confirming emission from two excited states. *J. Phys. Chem. A* **2001**, *105*, 1767−1771.
(20) Koti, A. S. R.; Periasamy, N. Application of time resolved area normalized emission spectroscopy to multicomponent systems. *J. Chem. Phys.* **2001**, *115*, 7094.
(21) Maroncelli, M.; Fleming, G. R. Picosecond solvation dynamics of coumarin 153: the importance of molecular aspects of solvation. *J. Chem. Phys.* **1987**, *86*, 6221.
(22) Moreno, F.; Cortijo, M.; González-Jiménez, J. Interaction of acrylodan with human serum albumin. A fluorescence spectroscopic study. *Photochem. Photobiol.* **1999**, *70*, 695−700.
(23) Lakowicz, J. R. *Principles of Fluorescence Spectroscopy*; Plenum Press: New York, 2006.
(24) Gore, S.; Velankar, S.; Kleywegt, G. J. Implementing an X-ray validation pipeline for the Protein Data Bank. *Acta Crystallogr., Sect. D: Biol. Crystallogr.* **2012**, *68*, 478−483.
(25) Gore, S.; Sanz García, E.; Hendrickx, P. M. S.; Gutmanas, A.; Westbrook, J. D.; Yang, H.; Feng, Z.; Baskaran, K.; Berrisford, J. M.; Hudson, B. P.; et al. Validation of structures in the Protein Data Bank. *Struct* **2017**, *25*, 1916−1927.
(26) Read, R. J.; Adams, P. D.; Arendall, W. B.; Brunger, A. T.; Emsley, P.; Joosten, R. P.; Kleywegt, G. J.; Krissinel, E. B.; Lütteke, T.; Otwinowski, Z.; et al. A new generation of crystallographic validation tools for the protein data bank. *Structure* **2011**, *19*, 1395−1412.
(27) Smart, O. S.; Horský, V.; Gore, S.; Svobodová Vařeková, R.; Bendová, V.; Kleywegt, G. J.; Velankar, S. Validation of ligands in macromolecular structures determined by X-ray crystallography. *Acta Crystallogr., Sect. D: Biol. Crystallogr.* **2018**, *74*, 228−236.
(28) Smart, O. S.; Horský, V.; Gore, S.; Svobodová Vařeková, R.; Bendová, V.; Kleywegt, G. J.; Velankar, S. Worldwide Protein Data Bank validation information: usage and trends. *Acta Crystallogr., Sect. D: Biol. Crystallogr.* **2018**, *74*, 237−244.
(29) Joosten, R. P.; Vriend, G. PDB improvement starts with data deposition. *Science* **2007**, *317*, 195−196.
(30) Joosten, R. P.; Salzemann, J.; Bloch, V.; Stockinger, H.; Berglund, A.-C.; Blanchet, C.; Bongcam-Rudloff, E.; Combet, C.; Da Costa, A. L.; Deleage, G.; et al. PDB_REDO: automated re-refinement of X-ray structure models in the PDB. *J. Appl. Crystallogr.* **2009**, *42*, 376−384.
(31) Joosten, R. P.; Womack, T.; Vriend, G.; Bricogne, G. Re-refinement from deposited X-ray data can deliver improved models for most PDB entries. *Acta Crystallogr., Sect. D: Biol. Crystallogr.* **2009**, *65*, 176−185.
(32) Trott, O.; Olson, A. J. AutoDock Vina: improving the speed and accuracy of docking with a new scoring function, efficient optimization, and multithreading. *J. Comput. Chem.* **2010**, *31*, 455−461.
(33) Mitra, P.; Pal, U.; Chandra Maiti, N.; Ghosh, A.; Bhunia, A.; Basu, S. Identification of modes of interactions between 9-amino-acridine hydrochloride hydrate and serum proteins by low and high resolution spectroscopy and molecular modeling. *RSC Adv.* **2016**, *6*, 53454−53468.
(34) Ghosh, N.; Mondal, R.; Mukherjee, S. Inverse Temperature Dependence in Static Quenching versus Calorimetric Exploration: Binding Interaction of Chloramphenicol to β-Lactoglobulin. *Langmuir* **2015**, *31*, 8074−8080.
(35) Zhang, X.; Keiderling, T. A. Lipid-induced conformational transitions of β-lactoglobulin. *Biochemistry* **2006**, *45*, 8444−8452.
(36) Bardhan, M.; Misra, T.; Ganguly, T. Quantization of bovine serum albumin by fluorescence enhancement effects and corresponding binding of macrocyclic host-protein assembly. *J. Photochem. Photobiol., B* **2012**, *106*, 113−119.
(37) Hasni, I.; Bourassa, P.; Tajmir-Riahi, H.-A. Binding of cationic lipids to milk β-lactoglobulin. *J. Phys. Chem. B* **2011**, *115*, 6683−6690.
(38) Valeur, B. *Molecular Fluorescence: Principles and Appplication*; Wiley-VCH Verlag GmbH: Weinheim, 2001.
(39) Patel, S.; Datta, A. Steady state and time-resolved fluorescence investigation of the specific binding of two chlorin derivatives with human serum albumin. *J. Phys. Chem. B* **2007**, *111*, 10557−10562.
(40) Barik, A.; Mishra, B.; Kunwar, A.; Indira Priyadarsini, K. Interaction of curcumin with human serum albumin: Thermodynamic properties, fluorescence energy transfer and denaturation effects. *Chem. Phys. Lett.* **2007**, *436*, 239−243.
(41) Portugal, C. A. M.; Crespo, J. G.; Lima, J. C. Anomalous "unquenching" of the fluorescence decay times of β-lactoglobulin induced by the known quencher acrylamide. *J. Photochem. Photobiol., B* **2006**, *82*, 117−126.
(42) Harvey, B. J.; Bell, E.; Brancaleon, L. A tryptophan rotamer located in a polar environment probes pH-dependent conformational changes in bovine β-lactoglobulin A. *J. Phys. Chem. B* **2007**, *111*, 2610−2620.
(43) Kinosita, K.; Ikegami, A.; Kawato, S. On the wobbling-in-cone analysis of fluorescence anisotropy decay. *Biophys. J.* **1982**, *37*, 461−464.
(44) Paul, B. K.; Guchhait, N. Modulation of Prototropic Activity and Rotational Relaxation Dynamics of a Cationic Biological Photosensitizer within the Motionally Constrained Bio-environment of a Protein. *J. Phys. Chem. B* **2011**, *115*, 10322−10334.
(45) Paul, B. K.; Ghosh, N.; Mukherjee, S. Direct insight into the nonclassical hydrophobic effect in bile salt:β-cyclodextrin interaction: role of hydrophobicity in governing the prototropism of a biological photosensitizer. *RSC Adv.* **2016**, *6*, 9984−9993.
(46) Quitevis, E. L.; Marcus, A. H.; Fayer, M. D. Dynamics of ionic lipophilic probes in micelles: picosecond fluorescence depolarization measurements. *J. Phys. Chem.* **1993**, *97*, 5762−5769.
(47) Kinosita, K.; Kawato, S.; Ikegami, A. A theory of fluorescence polarization decay in membranes. *Biophys. J.* **1977**, *20*, 289−305.
(48) Ahmad, B.; Parveen, S.; Khan, R. H. Effect of albumin conformation on the binding of ciprofloxacin to human serum albumin: a novel approach directly assigning binding site. *Biomacromolecules* **2006**, *7*, 1350−1356.
(49) Paul, B. K.; Ghosh, N.; Mukherjee, S. Binding Interaction of a Prospective Chemotherapeutic Antibacterial Drug with β-Lactoglobulin: Results and Challenges. *Langmuir* **2014**, *30*, 5921−5929.
(50) Ross, P. D.; Subramanian, S. Thermodynamics of protein association reactions: forces contributing to stability. *Biochemistry* **1981**, *20*, 3096−3102.
(51) Banerjee, S.; Dutta Choudhury, S.; Dasgupta, S.; Basu, S. Photoinduced electron transfer between hen egg white lysozyme and anticancer drug menadione. *J. Lumin.* **2008**, *128*, 437−444.
(52) Bent, D. V.; Hayon, E. Excited state chemistry of aromatic amino acids and related peptides. III. Tryptophan. *J. Am. Chem. Soc.* **1975**, *97*, 2612−2619.
(53) Creed, D. The photophysics and photochemistry of the near-UV absorbing amino acids−I. Tryptophan and its simple derivatives. *Photochem. Photobiol.* **1984**, *39*, 537−562.
(54) Chakraborty, B.; Basu, S. Magnetic Field Effect on Photo-induced Electron Transfer Reaction Associated with Hydrogen Bond Formation in Homogeneous Medium. *Appl. Magn. Reson.* **2012**, *42*, 5−15.
(55) Das, D.; Nath, D. N. Photoreaction of thioxanthone with indolic and phenolic derivatives of biological relevance: Magnetic field effect study. *J. Phys. Chem. A* **2008**, *112*, 11619−11626.
(56) Sengupta, T.; Dutta Choudhury, S.; Basu, S. Medium-Dependent Electron and H Atom Transfer between 2'-Deoxyadenosine and Menadione: A Magnetic Field Effect Study. *J. Am. Chem. Soc.* **2004**, *126*, 10589−10593.
(57) Zhao, G.-J.; Han, K.-L. Hydrogen bonding in the electronic excited state. *Acc. Chem. Res.* **2012**, *45*, 404−413.

https://dx.doi.org/10.1021/acs.langmuir.9b03506
Langmuir XXXX, XXX, XXX−XXX